# Could Effective Mechanical Properties of Soft Tissues and Biomaterials at Mesoscale be Obtained by Modal Analysis?

Pascal Swider, Yara Abidine, Pauline Assemat

# Could effective mechanical properties of soft tissues and biomaterials at mesoscale be obtained by modal analysis?

Pascal Swider[1*], Yara Abidine[1+], Pauline Assemat[1],
1 - IMFT UMR 5502, Toulouse University, Toulouse, France
*+ now at Transverse Laboratory Company*
Word count: 3459
Figure count: 3
Table count: 0
Keywords: soft biological tissue, biomaterial, modal analysis, vibration, mechanical properties, agarose, bone marrow

* Corresponding author:
Professor Pascal Swider
IMFT UMR 5502 CNRS - INPT - Toulouse 3
2 allées C. Soula, 31400 Toulouse cedex, France
Tel: +33 (0)561 497 944
Fax: +33 (0)561 496 745
e-mail: pascal.swider@imft.fr

**Abstract:**

**Background:** The mechanical properties of biological tissues and soft biomaterials are difficult to explore even though they play an important role in mechanobiological responses and organ homeostasis. Limited availability of harvested tissue and careful handling must be considered as well as discrepancies in biomaterial development.
**Objective:** We hypothesized that a mixed analytical-experimental modal analysis could be used to determine effective mechanical properties at the mesoscale for hydrated and fragile, poorly available and small-sized biological tissue and biomaterials.
**Methods:** Young's modulus $E$, shear modulus $G$ and Poisson's ratio $\nu$ were obtained from the measurement of first two natural frequencies of a set-up associating tested specimen with a cantilever. Tangent modules are calculated using a set of two analytical governing equations in linear vibration framework. A complementary parametric sensitivity analysis was performed. The methodology was evaluated using materials known to be challenging, namely agarose for biomaterials and bone marrow for biological tissues.
**Results:** Frequencies were in the range of 350 Hz and acquisition time of few seconds. Linear responses was checked and solution triplets ($E$, $G$, $\nu$) were ($99 \pm 10$ kPa, $43 \pm 0.3$ kPa, $0.16 \pm 0.1$) for agarose and ($61 \pm 12$ kPa, $28 \pm 7$ kPa, $0.07 \pm 0.03$) for bone marrow.
**Conclusion:** Comparisons with literature when available, confirmed approach acceptability. Limited influences of boundary conditions, brief experiments and reproducibility can be considered for applications to fragile and rare biomaterials and biological tissues, in addition to conventional characterization methods.

**List of symbols:**

$v(x,t)$, $w(x,t)$: transverse displacement of the cantilever

$Q(x,t)$, $M(x,t)$: shear force and bending moment in the cantilever

$\omega_i$, $\phi_i(x)$: angular frequency and mode shape

$E_cI$, $\rho_c$, $S$, $L$: cantilever properties: bending stiffness, density, cross- section, length

$E$, $G$, $\nu$: specimen properties: effective Young's modulus, shear modulus and Poisson's ratio

$\rho$, $\alpha$, $s$, $l$: specimen properties: density, shear coefficient, cross-section and length

$k$, $m$: specimen properties: translational stiffness and mass

$k_\theta$, $i_\theta$ : specimen properties: rotational stiffness and inertia

## I - Introduction

Human soft tissue mechanical properties determination is challenging because of tissue scarcity, frailty and underlying difficult handling, while they can play a significant role in tissue homeostasis [1, 2]. Pediatric pathologies and aging, traumatology and reconstruction, infection and oncology are strongly concerned by this issue [3 - 9]. Diagnosis, therapeutic strategies and patient follow-up could benefit from the knowledge of these properties.

The developments of innovative methodologies to identify in-vivo multiscale biophysical properties are still open issues. In-vivo techniques have been proposed including local indentation [10-13] or wave propagation, ultrasound elastography and MRI elastography at the macroscopic scale [14-18]. While those approaches are promising and are used to diagnose pathologies in some organs, the calculated elastic properties accuracy is still dependent upon the device resolution, upon the chosen mechanical model to evaluate the properties and upon the heterogeneities in the explored tissue. Limitations include also the depth at which the tissue is aimed to be explored for instance with ultrasound, the surrounding type of tissue such as bone or soft organs and the reproducibility of measurements (usage of manual probes).

Alternatively, ex-vivo soft tissue characterizations have been implemented since several decades while involving diversified modalities such as tensile, compressive and multiaxial tests or wave propagation - based tests [19 - 28] on diverse soft tissues such as brain, vessels, abdominal tissues, ligaments, fascia or skin. Non-linear governing equations frequently concern strain dependence and large deformation theory [19, 20, 21]. This complexity induces numerous identification models often based upon different strain energy function and involving series of coefficients fitted by using differentiated experimental characterization methodologies. Quasi-static response is frequently explored with robustness defined by domain depending upon stress and strain fields, displacement field or forces.

The availability of material in amount and size might be problematic [20, 29] and the intermediate mesoscopic scale (from mm to cm) between cell and macroscopic tissue can be relevant in clinical issue because of the spatial heterogeneity of tissues.

The modal analysis has been used to explore biological tissue properties [30 - 34]. At the macroscopic scale, it was often associated with numerical identification method to evaluate the uniqueness of distribution patterns and required delicate experimental procedures to obtain reliable modal bases. This approach finds limitations with small amount of material especially with soft and frailty tissues.

To contribute to this issue, we hypothesized that the analytical solutions of the two first mode shapes of a biological sample shaped in short cylinder and associated with a controlled cantilever could provide the effective mechanical properties of tissue, i.e. Young's modulus, shear modulus and Poisson's ratio, in one single measurement at the mesoscale. The proposed methodology is in

the field of linear vibrations which implies limited displacement and deformation fields in the vicinity of initial equilibrium position which allows to obtain the tangent moduli of the materials. This methodology could complement modalities often used sequentially such as tensile and shear tests and which can be very sensitive to boundary conditions and handling for hydrated and fragile, poorly available and small-sized tissue and biomaterials. The discriminant choice of tested materials was agarose for its compliance and bovine bone marrow explants for its significant compliance, fragility and problematic handling.

In this article, the theoretical modal analysis detailed initially, is followed by the description of the experimental methodology. The control specimens are agarose samples and the biological application concerned specimens of bovine bone marrow. To conclude, methodology discussions, limitations and perspectives are proposed.

## II – Theoretical and experimental methodology

### *2.1 Theoretical modal analysis*

When the clamped-free slender beam or cantilever described in Figure (1a) is considered, rectangular cross-section properties determine vertical plane (*O, x, y*) and horizontal plane (*O, x, z*) as principal bending vibration planes, associated with vertical displacement *v(x,t)* horizontal displacement *w(x,t)*. The tested cylindrical specimen considered as a short beam is located at the cantilever tip with a local reference frame defined by $(O,x_s,y_s,z_s)$. It respects the vertical symmetry plane such that local axis $x_s$ and $z_s$ are aligned with *y* and *z*, respectively.

The set of governing equations is detailed for the displacement in the vertical plane (*O, x, y*) and a similar methodology can be applied for the horizontal kinematics. The governing equation (1) described the conservative dynamic equilibrium of the cantilever beam in its motion *v*(*x,t*) with damping, shear and inertia effects of second order (Meirovitch 1986, Clough and Penzien 1975). The transverse displacement is written as the product of the mode shape $\phi(x)$ by the harmonic function *f(t)* with angular frequency $\omega$. Theoretical developments are detailed in Appendix.

$$E_c I \frac{\partial^4 v(x,t)}{\partial x^4} + \rho_c S \frac{\partial^2 v(x,t)}{\partial t^2} = 0 \quad \text{with} \quad v(x,t) = \phi(x) \cdot f(t) \tag{1}$$

Transverse displacement of the cantilever in the vertical plane induces a translation and an off-plane rotation of the specimen cross-section. Clamping conditions for $x = 0$ provides two kinematic equations. Two supplementary equations are obtained from the kinematics continuity at the specimen - cantilever interface, i.e. $x = L$. Local equilibrium on local axis $x_s$ give relationship, i.e. Equation (2a) between shear force *Q(L,t)* and translational dynamical force involving specimen translational stiffness *k* and mass *m*. Second, the cantilever bending moment *M(L,t)* is balanced by specimen dynamical moment depending upon rotational stiffness $k_\theta$ and mass inertia $i_\theta$ as expressed by equation (2b)

$$Q(L,t) - \left[k \cdot v(L,t) + m \cdot \ddot{v}(L,t)\right] = 0 \ \text{(a)} \ \text{ and } \ M(L,t) - \left[k_\theta \cdot \theta(L,t) + i_\theta \cdot \ddot{\theta}(L,t)\right] = 0 \ \text{(b)} \tag{2}$$

$$\text{with } Q(L,t) = -E_c I \frac{\partial^3 \phi(L)}{\partial x^3} \cdot f(t) \ \text{ and } \ M(L,t) = E_c I \frac{\partial^2 \phi(L)}{\partial x^2} \cdot f(t)$$

The determinant cancellation of matrix system (3) of boundary conditions is expressing the existence condition for a non-trivial solution for constants *C* to *F*. This transcendental equation involves natural frequencies $\omega$ known from experimental modal analysis.

$$\begin{bmatrix} 0 & 1 & 0 & 1 \\ 1 & 0 & 1 & 0 \\ (k-m\omega^2)\sin\beta L & (k-m\omega^2)\cos\beta L & (k-m\omega^2)\,\mathrm{sh}\beta L & (k-m\omega^2)\,\mathrm{ch}\beta L \\ +E_cI\beta^3\cos\beta L & -E_cI\beta^3\sin\beta L & -E_cI\beta^3\mathrm{ch}\beta L & -E_cI\beta^3\mathrm{sh}\beta L \\ (k_\theta - i_\theta\omega^2)\cos\beta L & -(k_\theta - i_\theta\omega^2)\sin\beta L & (k_\theta - i_\theta\omega^2)\,\mathrm{ch}\beta L & (k_\theta - i_\theta\omega^2)\,\mathrm{sh}\beta L \\ -E_cI\beta\sin\beta L & -E_cI\beta\cos\beta L & +E_cI\beta\,\mathrm{sh}\beta L & +E_cI\beta\,\mathrm{ch}\beta L \end{bmatrix} \begin{Bmatrix} C \\ D \\ E \\ F \end{Bmatrix} = \begin{Bmatrix} 0 \\ 0 \\ 0 \\ 0 \end{Bmatrix} \quad (3)$$

The similar methodology applied to the cantilever transverse displacement in the horizontal plane (*O, x, z*) is associating cantilever shear force to specimen dynamical translation force in $z_s$ and cantilever bending moment to specimen dynamical rotational moment in $x_s$. This is leading to the second transcendental equation.

Specimen contributes to kinetic energy and strain energy of the structure and unknown quantities introduced into expressions of *k*, *m*, $k_\theta$ and $i_\theta$ and appearing into transcendental equations are specimen effective material properties. Methodology to establish relationships between stiffness, mass, and material properties is based upon mechanics of curvilinear continuum and beam dynamics especially. Forces and moments are resulting from the product of interface motion, i.e. translation and off-plane rotation, by stiffness and mass matrix of the specimen. Specimen local reference frame (*O,* $x_s$*,* $y_s$*,* $z_s$). is detailed in Figure 1. Cubic approximation for transverse motion and linear approximation for longitudinal motion allow stiffness and mass matrices to be expressed explicitly after spatial integration. This is equivalent to considering a two-node finite element beam [Clough and Penzien 1975, Meirovitch et al. 1986, Blevins 2001, Lalanne et al. 1983] clamped at its base and attached to the cantilever tip. Stiffness coefficients are analytically exact while mass coefficients are approximated. To summarize, for the vertical mode shape, cantilever vertical motion *v(x,t)* is associated with longitudinal motion ($x_s$ axis) of the specimen and bending rotation around of the cantilever-specimen interface ($z_s$ axis). For the horizontal mode shape, cantilever horizontal motion *w(x,t)* is associated with transversal motion ($x_s$ axis) of the specimen and rotation around of the cantilever-specimen interface ($y_s$ axis). Translational stiffness *k* and mass *m*, rotational stiffness $k_\theta$ and inertia $i_\theta$ are involving effective Young's modulus *E*, shear modulus *G* and Poisson's ratio $\nu$. It can be noticed that for the vertical motion, translational stiffness *k* is only dependant upon *e* while rotational stiffness $k_\theta$ mainly influenced by *E*, is weighted by *G*. For the horizontal motion, *k* mainly influenced by *G*, is weighted by *E*.

Finally, transcendental equations involving stiffness and kinetic couplings are expressed by equations (8a) and (8b) for vertical and horizontal motions, respectively. Indeed, equation (8a) is a 3rd degree polynomial form in *E* coupled with linear terms in *G* whereas equation (8b) is a quadratic form in *G* associated with linear term in *E*. Coefficients $a_1$ to $a_{11}$ are detailed in appendix.

$$a_1\cdot e^3+\left(a_2\cdot g+a_3\right)\cdot e^2+\left(a_4\cdot g+a_5\right)\cdot e+a_6\cdot g=0 \quad \text{(a)} \qquad (8)$$

$$\left(a_7\cdot e+a_8\right)\cdot g^2+\left(a_9\cdot e+a_{10}\right)\cdot g+a_{11}\cdot e=0 \quad \text{(b)}$$

We targeted the two lowest first frequencies, i.e. the given $\beta_v$ and $\beta_h$, associated with vertical and horizontal mode shapes, i.e. $\phi_v$ and $\phi_h$, since they are predominant in the dynamical response. Among the six solutions (*E, G*) of equations (8a) and (8b) obtained using a Newton numerical scheme, only one was physically admissible. The admissible solution (*E, G*) put into system (7), give access to the dimensionless mode shape using Euclidean normalization. In addition, Poisson's ratio was deducted straightforwardly with $\nu = (E/2G)-1$ assuming an isotropic behavior of the specimen. Equation management and solving was managed using Maple software (MapleSoft®).

*2.2 Parametric sensitivity analysis*

The first order Taylor expansion of $E$ and $G$ for small variations of polynomial roots relative to vertical and horizontal mode shapes, allowed expressing dimensionless sensitivities of effective specimen properties to measured frequencies, i.e. $\beta_v$ and $\beta_h$. Sensitivity vector relative to $E$, i.e. $\mathbf{S}_E$, is detailed in equation (9) and those to $G$ and $\nu$, i.e. $\mathbf{S}_G$ and $\mathbf{S}_\nu$, were obtained similarly.

$$\mathbf{S}_E^t = \left( s_{E_v}, s_{E_h}, s_{E_{vh}} \right) \text{ with } s_{E_v} = \partial_{\beta_v} E \cdot \delta\beta_v / E \text{ , } s_{E_h} = \partial_{\beta_h} E \cdot \delta\beta_h / E \text{ and } s_{Evh} = \partial^2_{\beta_v \beta_h} E \cdot \delta\beta_v \cdot \delta\beta_h / E \quad (9)$$

First derivatives $\partial\beta$ were computed using a centred finite difference scheme on average solutions of system (8) and then, sensitivity vectors scaled using the Euclidean norm.

*2.3 Experimental modal analysis*

As shown in Figure (1), the 3D-printed fixture was associating the cantilever and a rigid and massive support compared with the cantilever and tested specimen. Cantilever geometrical properties were $L$ = 40.18 ± 0.04 mm, $b$ = 2.5 ± 0.07 mm and $h$ = 1.33 ± 0.08 mm. Material was a PLA polymer with $\rho_c$ = 1131 ± 0.8 kg/m$^3$ and $E_c$ = 2.5 $10^9$ ± 0.7 Pa. Cantilever mass and fixture mass including the fixation screw were $1.51.10^{-4}$ ± 0.1 kg and $1.3.10^{-2}$ ± 0.01 kg, respectively.

The set-up is described in Figure (2a) and Figure (2b). The tested specimen was located at the cantilever tip and maintained by a minimal drop of cyanoacrylate polymer for displacement continuity during vibration cycles. The fixture was mounted on an electrodynamic shaker (K2007E01; PCB® Piezotronics) using a piezoelectric force gauge (208C02; PCB® Piezotronics). In order to measure mode shapes in both vertical and horizontal plane, the cantilever is tilted on the support with an angle of 25° according to the support horizontal plane as seen on Figure (2c).

Natural frequencies were obtained from the frequency response function (FRF), as the ratio of the cantilever motion combining $v(\Omega)$ and $w(\Omega)$ over the excitation force $F(\Omega)$ in the frequency space [39,40]. The base displacement was monitored using a dynamic analyser (OR34; Oros®) with swept sine and random noise in the range 10 Hz - 1 kHz. Hanning window was used with 60 % overlap, 8192 FFT lines with sampling frequency up to 2 KHz. Minimal resolution in frequency was 0.24 Hz. Cantilever motion was measured using an optical displacement probe (confocal chromatic probe associated with CHRocodile 2S Precitec®) with a 12 µm spot diameter. A custom-made 3-axis motorized system using translation actuator (Newport®) was designed to identify the vertical and horizontal mode shapes $\phi(x,t)$ and automatize the displacement of the probe.

*2.4 Preparation of specimens*

Agarose as a derivative collagen was used initially to mimic biological tissue and evaluate the methodology. The 5% agarose gel (A0169 - 25G, Sigma-Aldrich) was prepared by mixing with deionized water and then placed at 4°C for one hour. Five molded cylindrical samples were used which dimensions were $d$ = 3.08 ± 0.15 mm in diameter and $l$ = 4.42 ± 0.15 mm in length. Specimen mass and density were $3.40\times10^{-5}$ ± 0.34 kg and $\rho$ = 1024 ± 1.7 kg/m$^3$, respectively.

Biological tissue was bone marrow harvested in bovine bone and five specimens were collected in the distal femoral epiphysis and metaphysis of three undifferentiated animals. Small cylindrical specimens were cut using a cylindrical hollow - punching device (Figure 2d). Cylinders were $d$ = 3.95 ± 0.2 mm in diameter and $l$ = 4.5 mm ± 0.23 mm in length. Specimen mass and density were $5.13\times10^{-5}$ ± 0.6 kg and $\rho$ = 1028.2 ± 5 kg/m$^3$. Tests were performed in laboratory air at room temperature of 21 ± 1°C.

Dimensions and masses were measured using a CCD laser micrometer (LS-7601, Keyence) and a precision balance (PPS413C Fisher Scientific®), respectively.

## 3 – Results

*Agarose specimen*

Averaged frequencies were obtained from three successive measurements of each specimen with a repeatability error of 2%. Averaged frequencies were 328 ± 12 Hz and 363 ± 4 Hz for the horizontal mode shape and vertical mode shape, respectively. Solution couples ($E$, $G$) were (99 ± 10 kPa, 43 ± 0.3 kPa) for agarose. Associated Poisson's ratio was 0.16 ± 0.1.

*Bone marrow specimen*

Averaged frequencies were 312 Hz ± 20 Hz for the vertical mode shape and 349 ± 9 Hz for the horizontal mode shape. Solution couples ($E$, $G$) were (61 ± 12 kPa, 28 ± 7 kPa) and Poisson ratio was $\nu = 0.07 \pm 0.03$.

An example of FRF Bode diagram is given Figure (2e). It shows two magnitude peaks at 250 Hz and 356 Hz and coinciding phase changings at 270°, i.e. $3\pi/2$. The presence of resonances associated with first vertical mode shape $\phi_v$ and first horizontal mode shape $\phi_h$ is confirmed. There is no difference between amplitude resonance and phase resonance which confirms the second order effect of structural damping. The linear responses were confirmed by ascending and descending swept sines giving reproducible magnitudes and phases, no inclination of magnitude peaks nor jump. Dimensionless mode shapes and are plotted in Figures (3b) and (3c), respectively.

*Sensitivity study*

For agarose the sensitivity vectors were $\mathbf{S}_E^{\,t}$ = (1, -0.005, 0) and $\mathbf{S}_G^{\,t}$ = (-0.17, 0.84, -0.001) and $\mathbf{S}_\nu^{\,t}$ = (0.35, -0.92, -0.006). For the bone marrow samples the sensitivity vectors were $\mathbf{S}_E^{\,t}$ = (1, -0.004, 0), $\mathbf{S}_G^{\,t}$ = (-0.16, 0.98, -0.001) and $\mathbf{S}_\nu^{\,t}$ = (0.37, -0.93, -0.007). Results showed that $E$ and $\beta_v$ were strongly correlated since $s_{Ev}$ was always predominant. Even if $G$ was playing the major role in the horizontal mode shape as shown by $s_{Gh}$ values, influences of vertical mode shape was not negligible. This effect increase when sensitivities of Poisson's ratio are studied. In all cases, crossed sensitivities, i.e. $s_{Evh}$, $s_{Gvh}$ and $s_{\nu h}$ had no effect.

## 4 – Discussion and Conclusion

We initially hypothesized that modal analysis could provide the effective elastic properties of soft tissue, especially for small and fragile specimens. In our approach, the multiphasic aspect of tissue was circumvented by the notion of effective properties and finally the millimetric mesoscopic scale was focused. Young modulus, shear modulus and Poisson ratio were obtained within the same analytical methodology nourished by the simultaneous measurement of two natural frequencies. This avoids numerical models such as FEM and inverse algorithms raising the discussion of convergence to a unique solution.

The experimental procedure took a few seconds without specific sample manipulation which is useful when exploring hydrated and fragile tissue or weakly available in amount. Indeed, natural frequencies are intrinsic to the structure whatever its scale and they can be revealed with minimal input energy while being measured with accuracy. The fixture was designed such that its mass and stiffness were much higher than those of specimen and cantilever. Their influence on overall ratio of kinetic by strain energy was negligible and did not affect targeted natural frequencies.

With conventional static tests, force boundary conditions might affect strain energy with significant local effects and tests must be designed accordingly with slender specimens, specific grips or enhanced modelling with identification inverse methods. In steady state dynamics, there is an energetic transfer between kinetic energy and strain energy so that the Lagrangian is constant.

This is the case when the structure is excited at resonance and responds throught associated mode shape. In our methodology resonance is measured without any contact force but using a foundation excitation with only minimal input energy and structure reveals its intrinsic response associating strain and mass effects. Indeed, kinetic energy due to distributed mass motion is associated with strain energy during a vibrational cycle. It helps compensating local effects of boundary conditions but also to smooth potentials effects of structural heterogeneities to provide effective material properties from natural frequencies. These are measured with great accuracy mainly due to fast acquisition of large numbers of time periods and robust post-treatment in frequency space. Obtaining material properties with unique testing modality and one single measurement sequence limits specimen handling and alteration especially for small and hydrated tissue.

Agarose was used as control and explored biological tissue was bovine bone marrow. For agarose, modal analysis and results from literature compare favorably in terms of magnitude orders [41 - 45]. Indeed, available values range between 10k Pa - 100 kPa and 2 kPa - 50 kPa for Young's modulus and shear modulus, respectively. Also, significant variations are inherent to material chemical composition, to specimen size and associated manufacturing process and to testing methods. Our results are more in the upper range of values. Used agarose gel was stiff enough to withstand tensile tests performed on molded shouldered test bars. The experimental methodology was not described because of its conventional character. Good comparison was obtained since discrepancies on Young's modulus were lower than 10%.

Concerning bone marrow, our results were also in agreement with the literature ranging from 1 kPa to 140 kPa for Young modulus and from 1 kPa to 200 kPa for shear modulus [2, 46 - 48]. When available, measures are strongly dependent upon investigation scales that are from cell to tissue with noticeable variations. Sources of significant discrepancies are attributed to the role of the extracellular matrix, hydration and temperature dependence or species and anatomic site associated with the collecting method [46]. Comparative tensile tests were unrealistic because of grip conditions. Compressive tests gave non-reproducible results due to deficiency of load-bearing structure and hydration loss incompatible with test durations.

In our methodology, Poisson's ratios were deducted from elastic moduli straightforwardly assuming isotropic properties. Averaged values were lower than 0.2 which confirmed the compressible nature of materials in the sense of continuous media mechanics and specifically biphasic or poroelastic behaviours [49 - 52]. Direct comparison with a documented literature was challenging since no data were available for either agarose or bone marrow, to our knowledge. Some values are however available for hydrogels of different macromolecules and generally less hydrated. They range between 0.3 and 0.5 with significant related to characterization methods. Nevertheless, magnitude order that we obtained was confirmed for biological tissue such as nucleus pulposus or meniscus with values comprises between 0.12 and 0.19 [55, 56].

The proposed methodology was primary oriented towards characterization of soft biomaterial and soft tissue available in limited amount. By adapting cantilever stiffness and mass, it can be applied to stiffer tissue such that cancellous bone such that specimen strain energy was playing a significant role into the modal response to highlight the role of effective material properties. Specimen shapes can also be modified depending upon in-vivo collection method even if it preferable to keep specimen axisymmetric properties to limit spatial couplings of mode shapes. For material without sufficient static stiffness such as fat tissue, a confinement system can be designed associated with specific developments of the dynamic analytical model.

The parametric sensitivity study showed that specimen Young's modulus and shear modulus were the prevailing factors into the vertical and horizontal mode shapes, respectively. This reinforces the validity of assumptions underlying our study. Compared with average values,

standard deviations were of the same magnitude order magnitude for both elastic modules, i.e. 20 % for agarose and 37 % for marrow. In return, they increased for Poisson ratios, i.e. 60 % for agarose and 95 % for marrow. Indeed, discrepeancies on Young's modulus and shear modulus were added when deriving Poisson's ratio. This was supported by intrinsic couplings revealed into the sensitivity vector and cumulative measurements uncertainties.

To highlight complementarity to conventional characterization methods, the proposed methodology has been evaluated using material, i.e agarose and bone marrow, which are challenging in term of mechanical characterization. Agarose studies circumvented material properties discrepancies using manufacturing process. In contrast bone marrow involved intrinsic variations due to animals and collecting sites. Here, the aim was to evaluate protocol feasibility and reproducibility without targeting an exhaustive exploration of tissue properties. Even if encouraging results have been collected, methodology relevance will be reinforced by testing a wider panel of materials, whether soft biological or substitute. Then, measuring of average properties of soft and fragile tissue population could be envisioned as well clinical biopsies from individual patients to quantify pathological responses.

Limitations could arise in joined theoretical and experimental aspects. First, the concept of equivalent elastic modulus underlying the proposed methodology can be discussed. Indeed, materials are multiphasic with the presence of a fluid phase saturating complex porous skeletons. Time-dependent properties at the microscale such as fluid-structure interactions or viscous properties of structural porous skeleton might provoke non-linear frequency dependence. However, response comparison of ascending and descending swept sines did not reveal effects of that type [39, 40]. Anyway, it can be kept in mind that tissue variability and uncertainties due sample preparation were always predominant.

Another limitation could concern the sample pre-stress condition which might affect effective modules because of non-linear effects. To that end, the initial conditions into the fixture verified a minimal contact positioning measured by cantilever initial deflection and much lower than the imposed vibrations. The linear response was confirmed by ascending and descending swept sines. However, the experimental device can easily be completed to mimic in-vivo non-linear responses by controlling initial imposed displacement and pre-stress of sample under the cantilever.

In conclusion, modal analysis showed compelling aspects for the identification of effective properties at the mesoscopic scale overall because of accuracy and reproducibility, limitation of boundary condition effects and short experimental time necessary for the measurement. It appears that the proposed theoretical and experimental procedure could be reasonably exploited to characterize fragile weakly available tissues or bioengineering materials which properties evolve rapidly in time.

**Acknowledgements:**
The French Minister of Education and Research, the French National Center for research (CNRS) and the Region Occitanie (France) are acknowledged for their assistance and financial support.

**Appendix :**

Under separation of variables hypothesis, the displacement *v(x,t)* is written as the product of the mode shape $\phi(x)$ by the time function *f(t)*. Verifying equation (1) gives conditions (A1) and (A2).

$$\frac{\partial^4\phi(x)}{\partial x^4} - \frac{\rho_c S}{E_c I}\cdot\omega^2\phi(x) = 0 \quad \text{(a)} \qquad \frac{\partial^2 f(t)}{\partial t^2} + \omega^2 f(t) = 0 \quad \text{(b)} \tag{A1}$$

Solutions of *f(t)* are harmonic functions with constants depending upon time initial conditions as expressed by equation (A2). The mode shape $\phi(x)$ is expressed by equation (A3a) with roots $\beta$ depending upon angular frequencies as detailed in (A3b).

$$f(t) = A\sin\omega t + B\cos\omega t \tag{A2}$$

$$\phi(x) = C\sin\beta x + D\cos\beta x + E\sinh\beta x + F\cosh\beta x \quad \text{(a)} \quad \text{with} \quad \beta = \left(\rho_c S\omega^2 / E_c I\right)^{1/4} \quad \text{(b)} \tag{A3}$$

Constants *C*, *D*, *E* and *F* depend on space boundary conditions. Clamping conditions in $x = 0$ give the two first equations (A4a) and (A4b) independent from *f*(t).

$$\phi(0) = 0 \ \text{(a)} \quad \text{and} \quad \frac{\partial\phi(0)}{\partial x} = 0 \ \text{(b)} \tag{A4}$$

For mode shapes describing motion in the vertical plane, i.e. *v*(*x*,*t*), mass and stiffness coefficients used in equation (8a) are detailed as follows:

$EI = E\,bh^3/12$, $m = \rho sl/3$, $i_\theta = \rho sl^3/105$, $k = es/l$, $k_\theta = (4+a)\,ei/(1+a)\,l$

with $i = s^2/4\pi$ and $a = 3es/\alpha\pi l^2 g$ with $\alpha$ : shear coefficient

For mode shapes describing motion in the horizontal plane, i.e. *w*(*x*,*t*), mass and stiffness coefficients used in equation (8b) are detailed as follows:

$EI = E.hb^3/12$, $m = 13\rho sl/35$, $i_\theta = \rho s^2 l/6\pi$, $k = 12\,ei/(1+a)\,l^3$, $k_\theta = gs^2/2\pi l$

with $i = s^2/2\pi$ and $a = 3es/\alpha\pi l^2 g$

In those equations, *b* and *h* are respectively the width and height of cantilever cross-section, *E* the cantilever Young's modulus. The parameters $\rho$, *s* and *l* are respectively the effective density, cross-section surface and length of the specimen whereas *e*, *g* and $\nu$ are the effective Young's modulus, the shear modulus and the Poisson's ratio of the specimen.

Coefficients of equations (8a) and (8b) are detailed as follows:

$$a_1 = 945s^4\left(1-\cos\beta L\,\mathrm{ch}\,\beta L\right) \qquad a_2 = 1260s^3\alpha\pi l^2\left(1-\cos\beta L\,\mathrm{ch}\,\beta L\right)$$

$$a_3 = -s^3\rho l^2\omega^2\left(315s+36\pi l^2\right)\left(1-\cos\beta L\,\mathrm{ch}\,\beta L\right)+945EI\beta^3 ls^3\left(\cos\beta L\,\mathrm{sh}\,\beta L+\sin\beta L\,\mathrm{ch}\,\beta L\right)$$
$$+3780EI\beta\pi ls^2\left(\cos\beta L\,\mathrm{sh}\,\beta L+\sin\beta L\,\mathrm{ch}\,\beta L\right)$$

$$a_4 = -s^3\rho l^2\omega^2\left(315s+36\pi l^2\right)\left(1-\cos\beta L\,\mathrm{ch}\,\beta L\right)+945EI\beta^3 ls^3\left(\cos\beta L\,\mathrm{sh}\,\beta L+\sin\beta L\,\mathrm{ch}\,\beta L\right)$$
$$+3780EI\beta\pi ls^2\left(\cos\beta L\,\mathrm{sh}\,\beta L+\sin\beta L\,\mathrm{ch}\,\beta L\right)$$

$$a_5 = -36\pi EI\beta^3 l^5 s^2\rho\omega^2\left(\cos\beta L\,\mathrm{sh}\,\beta L+\sin\beta L\,\mathrm{ch}\,\beta L\right)+1260\pi EI\beta l^3 s^2\rho\omega^2\left(\cos\beta L\,\mathrm{sh}\,\beta L-\sin\beta L\,\mathrm{ch}\,\beta L\right)$$
$$+3780\pi EI^2\beta^4 l^2 s\left(1+\cos\beta L\,\mathrm{ch}\,\beta L\right)+12\pi l^6 s^3\rho^2\omega^4\left(1-\cos\beta L\,\mathrm{ch}\,\beta L\right)$$

$$a_6 = -12\pi^2 EI\beta^3 l^7\alpha s\rho\omega^2\left(\cos\beta L\,\mathrm{sh}\,\beta L+\sin\beta L\,\mathrm{ch}\,\beta L\right)+420\pi^2 EI\beta l^5\alpha s\rho\omega^2\left(\cos\beta L\,\mathrm{sh}\,\beta L-\sin\beta L\,\mathrm{ch}\,\beta L\right)$$
$$+1260\pi^2 EI^2\beta^4 l^4\alpha\left(1+\cos\beta L\,\mathrm{ch}\,\beta L\right)+4\pi^2 l^3\alpha s^2\rho^2\omega^4\left(1-\cos\beta L\,\mathrm{ch}\,\beta L\right)$$

$$a_7 = 630\alpha s^4\left(1-\cos\beta L\,\mathrm{ch}\,\beta L\right)$$

$$a_8 = -39\pi\alpha s^3 l^4\rho\omega^2\left(1-\cos\beta L\,\mathrm{ch}\,\beta L\right)+105\pi\alpha s^2 EI\beta^3\left(\cos\beta L\,\mathrm{sh}\,\beta L+\sin\beta L\,\mathrm{ch}\,\beta L\right)$$

$$a_9 = -3\rho\omega^2 l^2 s^4\left(39+70\alpha\right)\left(1-\cos\beta L\,\mathrm{ch}\,\beta L\right)+315EI\beta^3 l s^3\left(\cos\beta L\,\mathrm{sh}\,\beta L+\sin\beta L\,\mathrm{ch}\,\beta L\right)$$
$$-1260EI\beta\pi l\alpha s^2\left(\cos\beta L\,\mathrm{sh}\,\beta L-\sin\beta L\,\mathrm{ch}\,\beta L\right)$$

$$a_{10} = -35\pi EI\beta^3 l^5\alpha s^2\rho\omega^2\left(\cos\beta L\,\mathrm{sh}\,\beta L+\sin\beta L\,\mathrm{ch}\,\beta L\right)+78\pi^2 EI\beta l^5\alpha s\rho\omega^2\left(\cos\beta L\,\mathrm{sh}\,\beta L-\sin\beta L\,\mathrm{ch}\,\beta L\right)$$
$$+210\pi^2 EI^2\beta^4 l^4\alpha\left(1+\cos\beta L\,\mathrm{ch}\,\beta L\right)+13\pi l^6 s^3\rho^2\omega^4\alpha\left(1-\cos\beta L\,\mathrm{ch}\,\beta L\right)$$

$$a_{11} = -105EI\beta^3 l^3 s^3\rho\omega^2\left(\cos\beta L\,\mathrm{sh}\,\beta L+\sin\beta L\,\mathrm{ch}\,\beta L\right)+234\pi EI\beta l^3 s^2\rho\omega^2\left(\cos\beta L\,\mathrm{sh}\,\beta L-\sin\beta L\,\mathrm{ch}\,\beta L\right)$$
$$+630\pi EI^2\beta^4 l^2 s\left(1+\cos\beta L\,\mathrm{ch}\,\beta L\right)+39l^4 s^4\rho^2\omega^4\left(1-\cos\beta L\,\mathrm{ch}\,\beta L\right)$$

**Ethical and conflict of interest statement:** The work described in the manuscript has not been published before. It is not under consideration for publication anywhere else, and the publication has been approved by all co-authors. The authors hereby declare to have no conflict of interest.

## References


1 - Humphrey JD, Dufresne ER, Schwartz MA (2014). Mechanotransduction and extracellular matrix homeostasis. Nat Rev Mol Cell Biol. 15(12):802-12.

2 - Lanske B, Rosen C (2017). Bone Marrow Adipose Tissue: The First 40 Years. J Bone Miner Res. 32(6):1153-1156.

3 - Roebuck DJ (1999). Skeletal complications in pediatric oncology patients. Radiographics. 19(4):873-85.

4 - Woo SL, Fisher MB, Feola AJ (2008). Contribution of biomechanics to management of ligament and tendon injuries. Mol Cell Biomech. 5(1):49-68.

5 - Watt AJ, Shin AY, Vedder NB, Chang J (2010). Joint arthritis and soft-tissue problems of the hand. Plast Reconstr Surg. 126(6):288e-300e.

6 - Choi J, Hoffman EA, Lin CL, Milhem MM, Tessier J, Newell JD Jr (2017). Quantitative computed tomography determined regional lung mechanics in normal nonsmokers, normal smokers and metastatic sarcoma subjects. PLoS One. 12(7):e0179812.

7 - Cortini M, Avnet S, Baldini N (2011). Mesenchymal stroma: Role in osteosarcoma progression. Cancer Lett. 405:90-99.

8 - Elkhenany HA, Szojka ARA, Mulet-Sierra A, Liang Y, Kunze M, Lan X, Sommerfeldt M, Jomha NM, Adesida AB (2021). Bone Marrow Mesenchymal Stem Cell-Derived Tissues are Mechanically Superior to Meniscus Cells. Tissue Eng Part A. 27(13-14):914-928.

9 - Meng KP, Majedi FS, Thauland TJ, Butte MJ (2020). Mechanosensing through YAP controls T cell activation and metabolism. J Exp Med. 217(8):e20200053.

10 - Lau A, Oyen ML, Kent RW, Murakami D, Torigaki T (2008). Indentation stiffness of aging human costal cartilage. Acta Biomater. 4(1):97-103.

11 - Jordan P, Kerdok AE, Howe RD, Socrate S (2011). Identifying a minimal rheological configuration: a tool for effective and efficient constitutive modeling of soft tissues. J Biomech Eng. 133(4):041006.

12 - Then C, Vogl TJ, Silber G (2012). Method for characterizing viscoelasticity of human gluteal tissue. J Biomech. 45(7):1252-8.

13 - Beccani M, Di Natali C, Sliker LJ, Schoen JA, Rentschler ME, Valdastri P (2014). Wireless tissue palpation for intraoperative detection of lumps in the soft tissue. IEEE Trans Biomed Eng. 61(2):353-61.

14 - Mariappan YK, Glaser KJ, Ehman RL. Magnetic resonance elastography: a review (2010). Clin Anat. 23(5):497-511.

15 - Wells PN, Liang HD (2011). Medical ultrasound: imaging of soft tissue strain and elasticity. J R Soc Interface. 8(64):1521-49.

16 - Sigrist RMS, Liau J, Kaffas AE, Chammas MC, Willmann JK (2017). Ultrasound Elastography: Review of Techniques and Clinical Applications. Theranostics. 7(5):1303-1329.

17 - Gennisson JL, Deffieux T, Fink M, Tanter M (2013). Ultrasound elastography: principles and techniques. Diagn Interv Imaging. 94(5):487-95.

18 - Gnyawali SC, Sinha M, El Masry MS, Wulff B, Ghatak S, Soto-Gonzalez F, Wilgus TA, Roy S, Sen CK (2020). High resolution ultrasound imaging for repeated measure of wound tissue morphometry, biomechanics and hemodynamics under fetal, adult and diabetic conditions. PloS One. 23;15(11):e0241831.

19 - Fung YC (1993). Biomechanics: Mechanical Properties of Living Tissues. Springer.

20 - Holzapfel GA, Ogden RW, Multiscale soft tissue mechanics and mechanobiology, 2018. Springer.

21 - Mihail LA, Goriely A. 2017, How to characterize a nonlinear elastic material? a review on nonlinear constitutive parameters in isotropic finite elasticity. Proc. R. Soc. A 473: 20170607.
20 - Miller K (2005). Method of testing very soft biological tissues in compression. J Biomech. 38(1):153-8.
21 - Gasser TC, Ogden RW, Holzapfel GA (2006). Hyperelastic modelling of arterial layers with distributed collagen fibre orientations. J R Soc Interface. 22;3(6):15-35.
22 - Pervin F, Chen WW (2009). Dynamic mechanical response of bovine gray matter and white matter brain tissues under compression. J Biomech. 16;42(6):731-5.
23 - Umale S, Deck C, Bourdet N, Dhumane P, Soler L, Marescaux J, Willinger R (2013). Experimental mechanical characterization of abdominal organs: liver, kidney & spleen. J Mech Behav Biomed Mater. 17:22-33.
24 - Nicolle S, Noguer L, Palierne JF (2013). Shear mechanical properties of the porcine pancreas: experiment and analytical modelling. J Mech Behav Biomed Mater. 26:90-7.
25 - Carniel EL, Rubini A, Frigo A, Natali AN (2014). Analysis of the biomechanical behaviour of gastrointestinal regions adopting an experimental and computational approach. Computer Methods and Programs in Biomedicine, 113(1):338–345.
26 - Disney CM, Lee PD, Hoyland JA, Sherratt MJ, Bay BK (2018). A review of techniques for modelling soft tissue microstructure deformation and quantifying strain Ex Vivo. J Microsc. 272(3):165-179.
27 - Guertler CA, Okamoto RJ, Schmidt JL, Badachhape AA, Johnson CL, Bayly PV (2018). Mechanical properties of porcine brain tissue in vivo and ex vivo estimated by MR elastography. J Biomech. 69:10-18.
28 - Van Haaften EE, van Turnhout MC, Kurniawan NA (2019). Image-based analysis of uniaxial ring test for mechanical characterization of soft materials and biological tissues. Soft Matter. 15(16):3353-3361.
29 - Duck FA (1990). Physical properties of tissue. Academic Press.
30 - Swider P, Guérin G, Baas J, Søballe K, Bechtold JE (2009). Characterization of bone-implant fixation using modal analysis: application to a press-fit implant model. J. Biomech. 42, 1643–1649.
31 - Scholz R, Hoffmann F, von Sachsen S, Drossel WG, Klöhn C, Voigt C (2013). Validation of density-elasticity relationships for finite element modelling of human pelvic bone by modal analysis. J. Biomech. 46, 2667–2673.
32 - Miyashita M, Ogawa T, Naito H, Shibamoto A, Wang AS, Shobara K, Sasaki K (2018). Evaluation of implant screw loosening by resonance frequency analysis with triaxial piezoelectric pick-up: in vitro model and in vivo animal study. Clin Oral Investig. 22(5):2129-2134.
33 - Henyš P, Čapek L (2019). Computational modal analysis of a composite pelvic bone: convergence and validation studies. Comput Methods Biomech Biomed Engin. 22(9):916-924.
34 - Blondel M, Abidine Y, Assemat P, Palierne S, Swider P (2020). Identification of effective elastic modulus using modal analysis; application to canine cancellous bone. J Biomech. 18;110:109972.
35 - Meirovitch L (1986). Elements of vibration analysis, 2nd edition. McGraw-Hill, USA.
36 - Clough RW, Penzien J (1975). Dynamics of structures, McGraw-Hill. USA.
37 - Blevins RD (2001). Formulas for natural frequency and mode shape. Krieger publishing company.
38 - Lalanne M, Berthier P, Der Hagopian J (1983). Mechanical vibrations for engineers. Wiley and Sons.
39 - Nashif AD, Jones DI, Henderson JP (1985). Vibration damping. Wiley, USA.
40 - Ewins DJ (2000). Modal Testing; theory, practice and application. 2nd edition, Wiley, USA.

41 - Xia T, Liu W, Yang L (2017). Agarose properties. A review of gradient stiffness hydrogels used in tissue engineering and regenerative medicine. J Biomed Mater Res A. 105(6):1799-1812.
42 - Salati MA, Khazai J, Tahmuri AM, Samadi A, Taghizadeh A, Taghizadeh M, Zarrintaj P, Ramsey JD, Habibzadeh S, Seidi F, Saeb MR, Mozafari M (2020). Agarose-Based Biomaterials: Opportunities and Challenges in Cartilage Tissue Engineering. Polymers. 12(5):1150.
43 - Gao X, Gu W (2014). A new constitutive model for hydration-dependent mechanical properties in biological soft tissues and hydrogels. J Biomech. 47(12):3196-200.
44 - Gross W, Kress H (2017). Simultaneous measurement of the Young's modulus and the Poisson ratio of thin elastic layers. Soft Matter. 13(5):1048-1055.
45 - Sadeghi S, Cortes DH (2020). Measurement of the shear modulus in thin-layered tissues using numerical simulations and shear wave elastography. J Mech Behav Biomed Mater. 102:103502.
46 - Metzger TA, Shudick JM, Seekell R, Zhu Y, Niebur GL (2014). Rheological behavior of fresh bone marrow and the effects of storage. J Mech Behav Biomed Mater. 40:307-313.
47 - Jansen LE, Birch NP, Schiffman JD, Crosby AJ, Peyton SR (2015). Mechanics of intact bone marrow. J Mech Behav Biomed Mater. 50:299-307.
48 - Curtis KJ, Oberman AG, Niebur GL (2020). Effects of mechanobiological signaling in bone marrow on skeletal health. Ann N Y Acad Sci. 1460(1):11-24.
49 - Cowin SC (1999). Bone poroelasticity. J. Biomech. 32(3):217-38.
50 - Coussy O (2004). Poromechanics, Wiley, USA.
51 - Ehret A E, Bircher K, Stracuzzi A, Marina V, Zündel M, Mazza E (2017). Inverse poroelasticity as a fundamental mechanism in biomechanics and mechanobiology. Nat Commun. 17;8(1).
52 - Esteki MH, Alemrajabi AA, Hall CM, Sheridan GK, Azadi M, Moeendarbary E (2020). A new framework for characterization of poroelastic materials using indentation. Acta Biomater. 102:138-148.
53 - Zhang W, Soman P, Meggs K, Qu X, Chen S (2013). Tuning the Poisson's Ratio of Biomaterials for Investigating Cellular Response. Adv Funct Mater. 23(25):10.1002/adfm.201202666.
54 - Cappello J, d'Herbemont V, Lindner A, du Roure O (2020). Microfluidic In-Situ Measurement of Poisson's Ratio of Hydrogels. Micromachines. 19;11(3):318.
55 - Normand V, Lootens DL, Amici E, Plucknett KP, Aymard P. New insight into agarose gel mechanical properties. Biomacromolecules. 2000, 1(4):730-8.
56 - Farrell MD, Riches PE (2013). On the poisson's ratio of the nucleus pulposus. J Biomech Eng. 135(10):104501.
57 - Danso EK, Julkunen P, Korhonen RK (2018). Poisson's ratio of bovine meniscus determined combining unconfined and confined compression. J Biomech. 22;77:233-237.

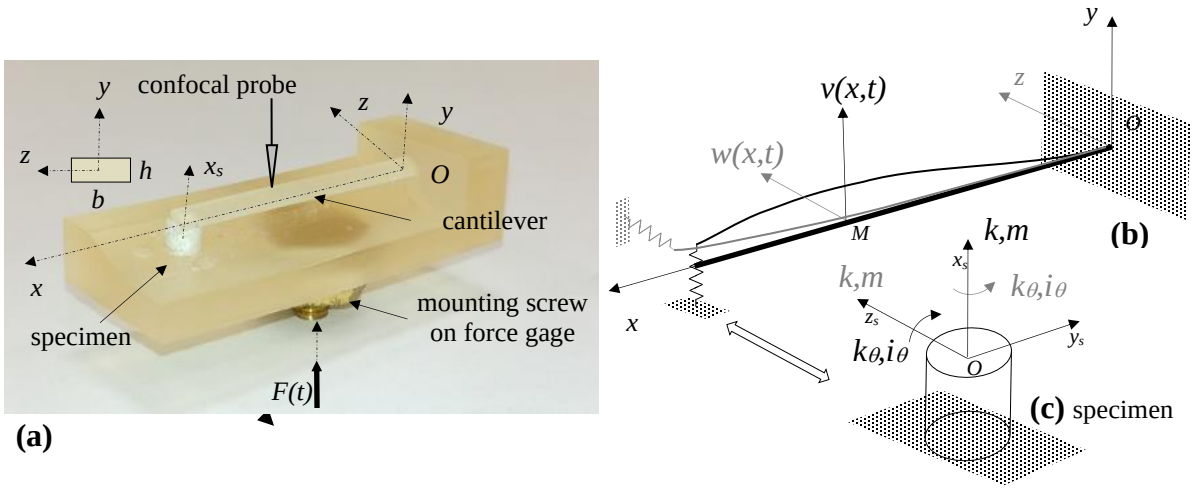


**Figure 1 – (a)** Experimental device: clamped beam simply supported on the elastic specimen with (*O*,*x*,*y*,*z*) being the cantilever reference frame. **(b)** Diagram of the theoretical model: *v(x,t)* is the cantilever transversal displacement in the vertical plane *(O,x,y)* and *w(x,t)* is the cantilever transversal displacement in the horizontal plane *(O,x,z)*. **(c)** Specimen stiffness and mass properties: *k*, $k_\theta$, *m* and $i_\theta$ are involved into the dynamic vertical response (—) and *k*, $k_\theta$, *m* and $i_\theta$ are involved into the dynamic horizontal response (—). The excitation force is *F(t)*.

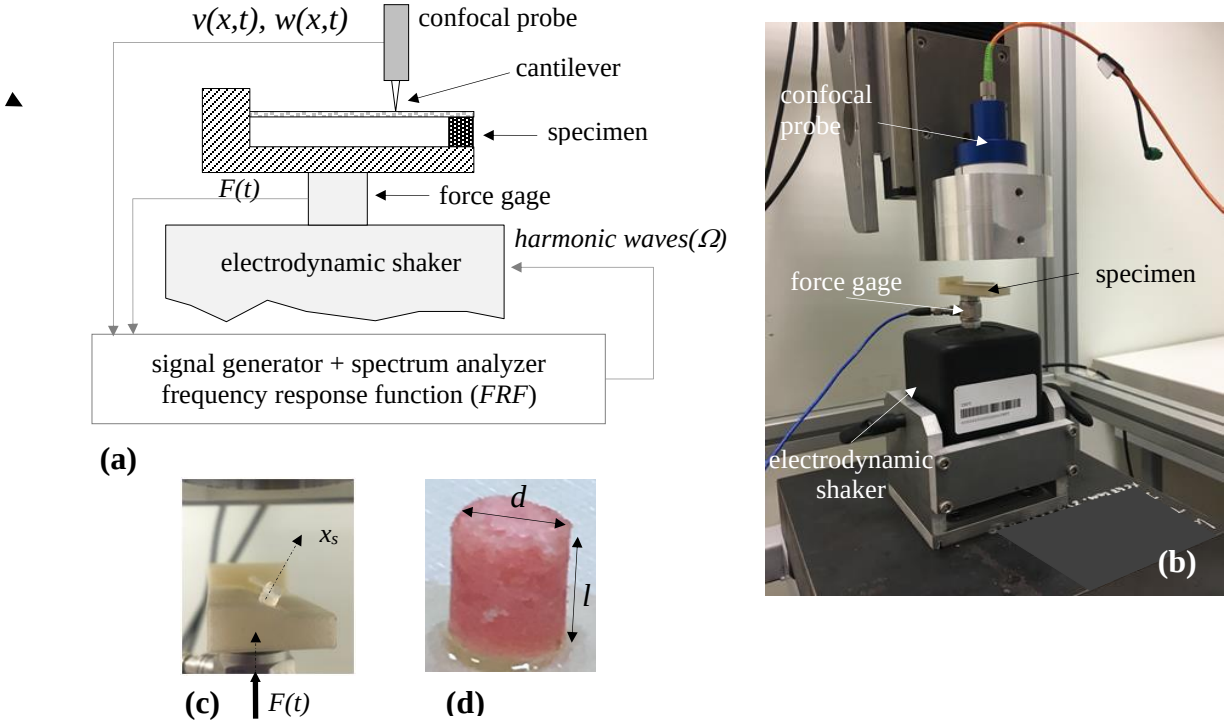


**Figure 2 – (a)** Diagram of the experimental device, **(b)** Experimental set-up, **(c)** Agarose specimen in the fixture, **(d)** Bone marrow specimen

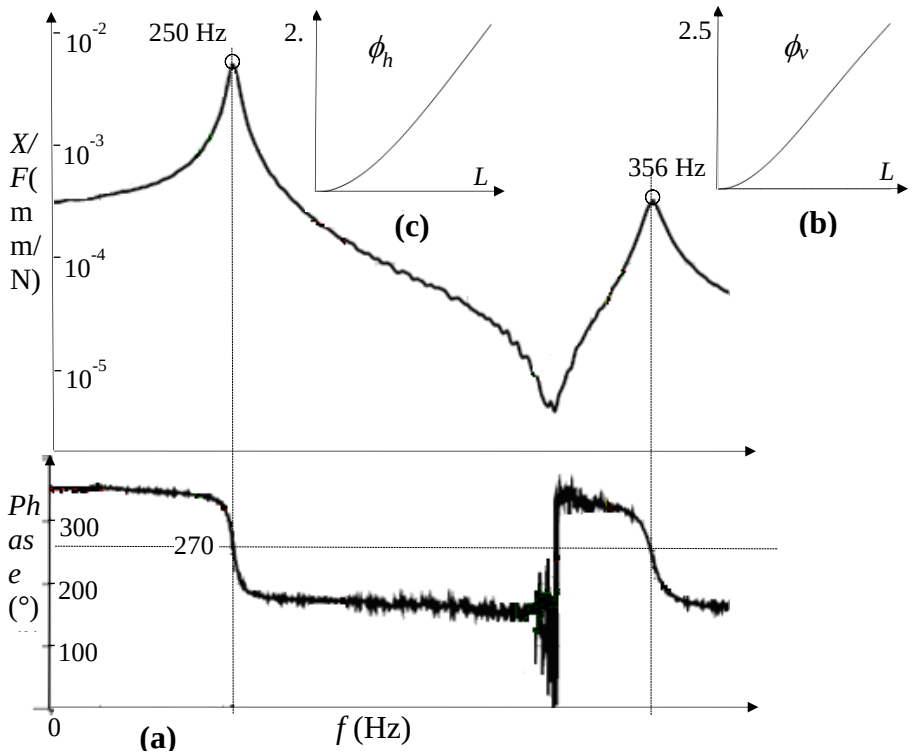


**Figure 3 – Frequency response function of the structure (agarose specimen and cantilever): (a)** Bode representation, i.e. *X/F* in magnitude (mm/N) and phase (°), *X* being the displacement magnitude measured by the confocal probe and *F* the transmitted force magnitude, **(b)** dimensionless first mode shape $\phi v$ (frequency: 250 Hz) in the vertical plane *(O,x,y)*, **(c)** dimensionless first horizontal mode shape $\phi_h$ (frequency : 356 Hz) in the horizontal plane *(O,x,z)*.